



## Solar Photocatalytic Activity of Nanocrystalline ZnO Obtained from Different Precursors

I.S. QURAISHI<sup>1,2</sup>, R.A. PAWAR<sup>1,2</sup>, D.R. SHINDE<sup>1,\*</sup>, P.S. TAMBADE<sup>1</sup> and M.G. CHASKAR<sup>1</sup>

<sup>1</sup>Department of Chemistry, P.D.E.A's Prof. Ramkrishna More College, Akurdi, Pune-411044, India

<sup>2</sup>Research Center in Chemistry, Baburaoji Gholap College, Sangvi, Pune-411027, India

\*Corresponding author: E-mail: drshindechemistry1970@gmail.com

Received: 2 November 2019;

Accepted: 15 January 2020;

Published online: 29 April 2020;

AJC-19847

In present study, ZnO photocatalysts were successfully synthesized by thermal decomposition of different precursors. Thermal decomposition temperatures of precursors were obtained by thermogravimetric analysis. The synthesized ZnO photocatalysts were characterized for their crystalline phase, surface morphology and band gap, respectively by powder X-ray diffraction, scanning electron microscopy and diffuse reflectance spectroscopic methods. Chemical analysis of synthesized ZnO photocatalysts was performed for Zn(II) content. Photocatalytic activity of ZnO photocatalysts was evaluated under the solar irradiation on crystal violet dye in aqueous solution. The results of experiments showed that ZnO synthesized from zinc carbonate consists of higher photocatalytic activity than ZnO synthesized from other precursors, which is even higher than bench mark Degussa P-25 TiO<sub>2</sub> photocatalyst. ZnO synthesized from zinc carbonate is further used for mineralization of dyes from three different effluents.

**Keywords:** Zinc oxide, Photocatalysis, Crystal violet, Degradation.

### INTRODUCTION

Nanocrystalline metal oxides were reported as potential materials for the photocatalytic mineralization of organic pollutants in water [1,2]. Among the various metal oxides, nanocrystalline ZnO has been reported as promising photocatalyst owing to its unique optical properties such as high direct band gap (3.2 eV), large excitation binding energy (60 meV), high activity in visible light than other metal oxides and good photostability [3-5]. In literature, several methods were reported for the synthesis of ZnO photocatalyst. Some of the frequently employed methods are sol-gel, dry chemical milling, thermal decompositions of precursors, wet precipitation, combustion, hydrothermal, and template assisted synthesis [1,2,6-10].

Some of these methods are highly useful to obtain pure nanocrystalline ZnO having specific grain structures. However, they are expensive, time consuming and also requires lots of energy. Therefore, they cannot be employed for the large scale production of ZnO photocatalyst. Therefore, there is a need to obtain photocatalyst grade ZnO by low cost method. Among the various methods, thermal decomposition of precursors is the simplest methods for synthesis of photocatalyst grade ZnO. Moreover, this method can be easily adopted for large scale

and cost effective production of photocatalyst grade ZnO. Thus, in present study a comparative account of photocatalytic activity of ZnO obtained from different precursors were analyzed. The precursors selected were zinc oxalate, zinc tartarate, zinc carbonate, basic zinc carbonate and zinc peroxide. The photocatalysts were characterized by appropriate methods and their photocatalytic activity was evaluated and compared on the crystal violet dye as a model organic compound.

### EXPERIMENTAL

Analytical reagent grade zinc acetate, tartaric acid, conc. ammonia, 30% H<sub>2</sub>O<sub>2</sub>, basic zinc carbonate and other chemicals were procured from Loba Chemie Pvt. Ltd. and used without further purifications.

**Synthesis of ZnO photocatalysts:** ZnO photocatalysts were synthesized by thermal decompositions of five different precursors *viz.* zinc carbonate, basic zinc carbonate, zinc oxalate, zinc peroxide and zinc tartarate. Zinc oxalate, zinc tartarate and zinc peroxide were synthesized by prescribed methods discussed elsewhere [11,12]. Zinc tartarate was prepared similarly as that of zinc oxalate where oxalic acid in the reaction was replaced by tartaric acid. Zinc carbonate was prepared by

precipitation method. The aqueous solution of zinc acetate (0.1M, 500 mL) was prepared and pH was adjusted to 9 by adding concentrated ammonia at 60 °C. In this solution, 50 mL of 2M ammonium carbonate was added dropwise with constant magnetic stirring. This resulted in the formation of white precipitate which was then filtered through Whatman filter paper 42. The filtered precipitate washed with distilled water and then with ethanol. Decomposition pattern of all precursors in air to form ZnO was studied by thermogravimetric analysis (TGA) method. All the precursors were dried in an oven for 1 h at 90 °C and appropriate quantity was transferred in a silica crucible. The precursor was decomposed by heating on Bunsen burner in open crucible. The decomposition product of each precursor was then annealed in a muffle furnace at predetermined temperature and time which resulted in the formation of desired ZnO photocatalyst. The benchmark catalyst Degussa P-25 TiO<sub>2</sub> was obtained from nano-shell and used in the present study.

**Characterisation of ZnO nanoparticles:** All ZnO photocatalysts were analyzed for Zn(II) content by volumetric method [13]. The crystalline phase, surface morphology and band gap of each synthesized ZnO was studied respectively by powder X-ray diffraction (XRD) method, scanning electron microscopic (SEM) imaging and UV-visible diffuse reflectance spectra (UV-DRS). The UV-visible absorption characteristics of synthesized ZnO samples in aqueous solution were obtained by recording absorption spectra. The specific surface area was calculated by the prescribed method from the crystallite size and powder density [14,15].

**Evaluation of photocatalytic activity:** Crystal violet was used as a model organic pollutant to evaluate the photocatalytic activity of ZnO nanoparticles. The photocatalytic degradation experiments were conducted in the sunlight on sunny days between 10 am to 3 pm when the sunlight intensity was in the range of 56,900 to 65,800 lux. Crystal violet dye solution with appropriate concentration (10 mg L<sup>-1</sup>) was prepared in the water and stored in the dark. Stability of dye in an aqueous solution in the dark in presence of ZnO as well as in the light in absence of ZnO at pH 5 to 9 was studied before the photocatalytic degradation experiments. The photocatalytic experiments were executed in a flat slurry reactor as described by Shinde *et al.* [2]. The first order rate constant was calculated by Langmuir-Hinshelwood equation [16] (eqn.1):

$$k_{\text{obs}} = \frac{2.303}{t} \log \left( \frac{A_0}{A_t} \right) \quad (1)$$

where;  $k_{\text{obs}}$  = rate constant,  $A_0$  = initial absorbance of dye solution,  $A_t$  = absorbance of dye solution at time  $t$ .

After studying the photocatalytic degradation of crystal violet using ZnO particles synthesized using five different precursors, the best one was selected for further study. Photocatalytic mineralization of dyes from three effluents was achieved using the best ZnO catalyst. The dye effluents were collected from small scale fabric dyeing unit located at Malegaon city, India. The chemical oxygen demand (COD) of a treated dye solution was determined by the prescribed method [13].

## RESULTS AND DISCUSSION

**Thermal analysis:** Thermogravimetric analysis of precursors was performed to obtain decomposition temperature which also confirmed the formation of specific precursor. TG curves analysis (Fig. 1) showed that zinc carbonate and basic zinc carbonate decompose completely below 300 °C to form ZnO while zinc oxalate and zinc tartarate decomposed respectively at 430 and 560 °C. The molecular formulae were confirmed from TG analyses and recorded in Table-1. The TG analysis of zinc peroxide is not possible as it decomposes violently. However, we have obtained its decomposition temperature manually and decomposes nearly at 210 °C.

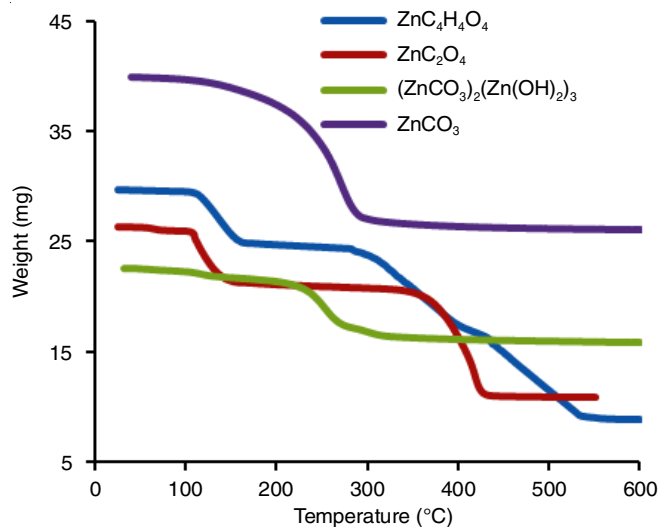


Fig. 1. TG curves of ZnO precursors

**Characteristics of ZnO precursors:** Zinc(II) content in synthesized ZnO using different precursors (Table-1) was obtained by the chemical method of analysis and found to be in good agreement with the molecular formula of ZnO which revealed the high purity of all ZnO photocatalysts.

Crystallite properties of ZnO photocatalysts were confirmed from their powder XRD patterns (Fig. 2). The powder XRD of all ZnO photocatalysts consist of sharp and intense

TABLE-1  
TG ANALYSIS PRECURSORS AND Zn(II) CONTENT IN ZnO SAMPLES OBTAINED FROM DIFFERENT PRECURSORS

Precursor	m.f.	Decomposition temperature (°C)	Abbreviation to ZnO sample	Zn(II) content (%)
Zinc oxalate	ZnC <sub>2</sub> O <sub>4</sub> ·2H <sub>2</sub> O	430	ZnO <sub>ox</sub>	79.11 ± 0.52
Zinc tartarate	ZnC <sub>4</sub> H <sub>4</sub> O <sub>4</sub> ·2H <sub>2</sub> O	560	ZnO <sub>tar</sub>	79.36 ± 0.31
Zinc carbonate	ZnCO <sub>3</sub>	280	ZnO <sub>car</sub>	79.56 ± 0.56
Basic zinc carbonate	(ZnCO <sub>3</sub> ) <sub>2</sub> (Zn(OH) <sub>2</sub> ) <sub>3</sub>	300	ZnO <sub>bcar</sub>	79.12 ± 0.31
Zinc peroxide	ZnO <sub>2</sub>	210	ZnO <sub>perox</sub>	80.08 ± 0.30

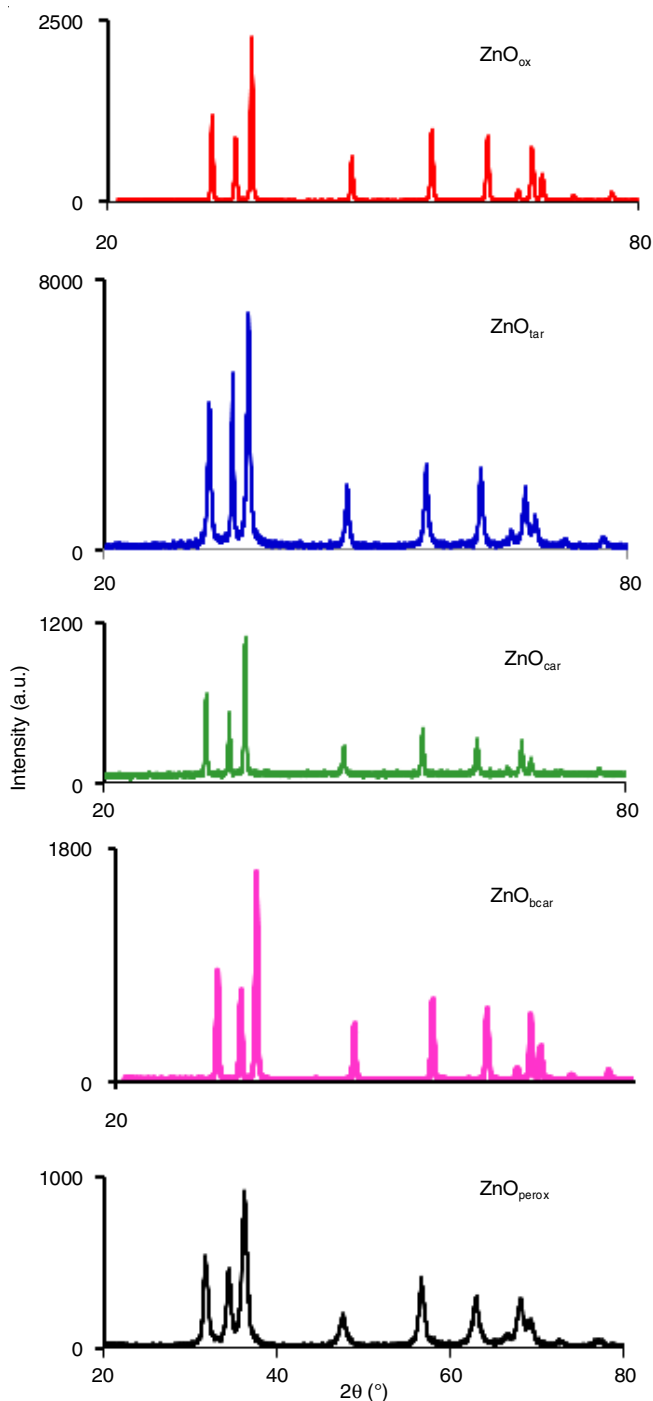


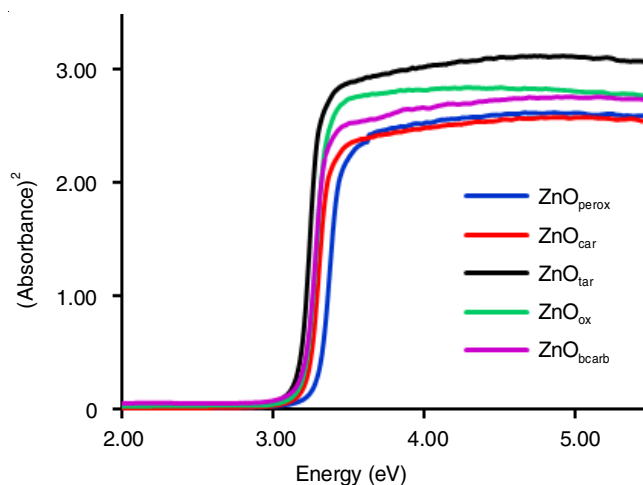
Fig. 2. Powder XRD of ZnO photocatalysts

peaks representative of their high crystalline nature. The peaks in XRD can be indexed to the plans [100], [002], [101], [102], [110], [103], [200], [112] and [201] of ZnO crystal. All the photocatalyst showed peak positions at similar diffraction angle

in XRD and they match with JCPDS data file number 36-1451 of ZnO having hexagonal crystalline structure. From the observed powder XRD patterns, different crystal parameters (unit cell parameters, crystal volume, crystal density, Zn-O bond length) were calculated (Table-2) and found in agreement with JCPDS data file number 36-1451 of ZnO. Furthermore, powder XRD of any of photocatalyst did not exhibit extra peak other than the hexagonal crystalline phase of ZnO, which further confirmed high purity of their crystalline phase.

The results of powder XRD of ZnO photocatalysts were analogous with previously reported XRD pattern for nanocrystalline ZnO [17-19]. Crystallite sizes of ZnO samples were calculated using Debye-Scherrer's equation and found be different for all five ZnO photocatalysts (Table-2).

**Band gap of ZnO:** Band gaps of ZnO photocatalysts were obtained from the diffuse reflectance spectra in the absorbance mode. From the obtained data, the graph of (absorbance)<sup>2</sup> against the energy of radiation (eV) was plotted (Fig. 3) and band gaps were obtained. The band gaps of photocatalysts were found in the range of 3.16 to 3.27 eV. The observed band gaps were consistent with previously reported values of nanocrystalline ZnO photocatalysts [20,21].

Fig. 3. Graph of (absorbance)<sup>2</sup> against energy (eV) of radiations

The light absorption characteristics of ZnO photocatalysts were studied by recording absorbance spectra (Fig. 4) of ZnO suspension in water. All the ZnO photocatalysts showed an absorption maxima in the range of 369 to 386 nm, which belong to valence to conduction band excitation of electron *i.e.* band gap of ZnO sample. Small variation arises in absorption maxima due to the small variation of crystallite size of ZnO. This observation indicates that all the ZnO photocatalysts absorbed near to the visible region and consist of small absorbance of radiations in the visible region.

TABLE-2  
POWDER XRD CHARACTERISTICS OF ZnO PHOTOCATALYSTS

ZnO Sample	a (Å)	c (Å)	Unit cell volume (Å) <sup>3</sup>	X-ray density (gcm <sup>-3</sup> )	Zn-O bond length (Å)	Crystallite size (nm)	Specific surface area (m <sup>2</sup> g <sup>-1</sup> )
ZnO <sub>ox</sub>	3.2478	5.2022	47.5212	5.6872	1.9764	27.58	111.21
ZnO <sub>tar</sub>	3.2483	5.2031	47.5500	5.6838	1.9768	32.74	92.75
ZnO <sub>car</sub>	3.2483	5.2081	47.5902	5.6790	1.9774	21.57	142.36
ZnO <sub>bcarb</sub>	3.2467	5.2048	47.5123	5.6883	1.9759	22.36	136.35
ZnO <sub>perox</sub>	3.2457	5.2066	47.4998	5.6898	1.9761	12.06	249.38

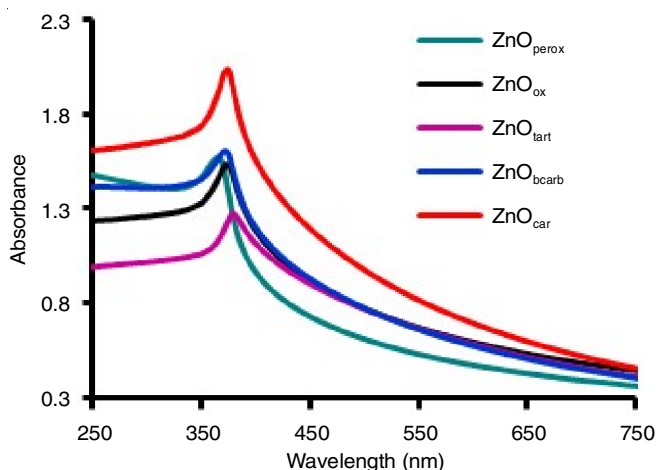


Fig. 4. UV-visible absorbance spectra of ZnO photocatalysts in aqueous solution

**Particle morphology:** The particle morphologies of ZnO photocatalysts were examined by SEM imaging (Fig. 5). The SEM image of ZnO<sub>perox</sub> showed a high level of agglomeration of small spherical particles to form large clusters. The grains of ZnO<sub>ox</sub> were irregular in shape and showed a coexistence of ZnO crystallites to form large agglomerates. Among the five ZnO photocatalysts, grains of ZnO<sub>car</sub> and ZnO<sub>bcarb</sub> were elliptical to globular in shape and consist of porous surface. The grains of these two samples showed a separate existence. The grains of ZnO<sub>tar</sub> photocatalyst were irregular in shape, larger in size and showed a individual existence.

**Photoluminescence characteristics:** Photoluminescence spectra of ZnO photocatalysts (Fig. 6) exhibited a first emission peaks at 380 to 392 nm, which belongs to band gap emission of ZnO. Other peaks which were present in visible region could be attributed to defects in crystal structure of ZnO crystallites [22,23]. The major difference in photoluminescence spectra is of ZnO<sub>perox</sub> photocatalyst which displayed a high intensity peak in visible region. It might be due to smaller crystallite

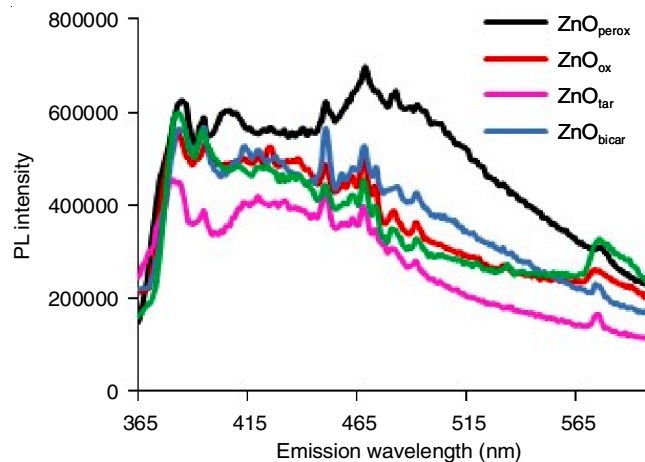


Fig. 6. PL spectra of ZnO photocatalysts

size of this sample since smaller crystallites are more defective in nature.

**Comparison of photocatalytic activity of ZnO photocatalysts:** The photocatalytic activity of each synthesized ZnO was evaluated in terms of rate constant of decolorization of crystal violet as a model dye compound. The pseudo first-order rate constant of decolorization reaction of crystal violet dye was evaluated under optimized reaction conditions (pH 9, catalyst dose 0.4 g L<sup>-1</sup>). The graph of log(A<sub>0</sub>/A<sub>t</sub>) against time is almost straight line passing through the origin (R<sup>2</sup> > 0.95; Fig. 7). The pseudo first-order rate constant (k) was calculated from the slope of line. The highest rate constant of decolorization of crystal violet dye was observed with ZnO<sub>car</sub> photocatalyst (0.094 min<sup>-1</sup>). For other ZnO photocatalysts, the rate constant of decolorization were 0.087, 0.068, 0.064 and 0.062 min<sup>-1</sup>, respectively with ZnO<sub>bcarb</sub>, ZnO<sub>ox</sub>, ZnO<sub>perox</sub> and ZnO<sub>tar</sub>. Under the optimized condition (pH = 7), a quantity of Degussa P-25 TiO<sub>2</sub> (400 mg L<sup>-1</sup>) and the height of effluent in reactor, the rate constant for decolorization of the crystal violet dye was found to be 0.071 min<sup>-1</sup>.

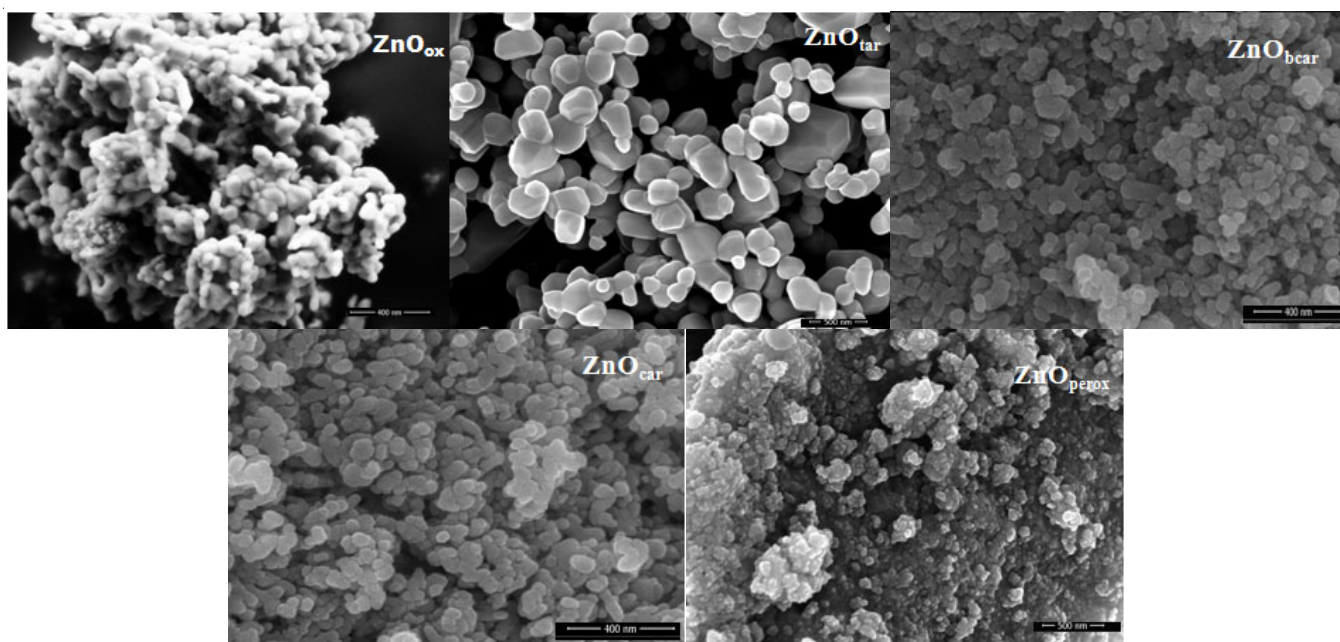


Fig. 5. SEM images of ZnO photocatalysts

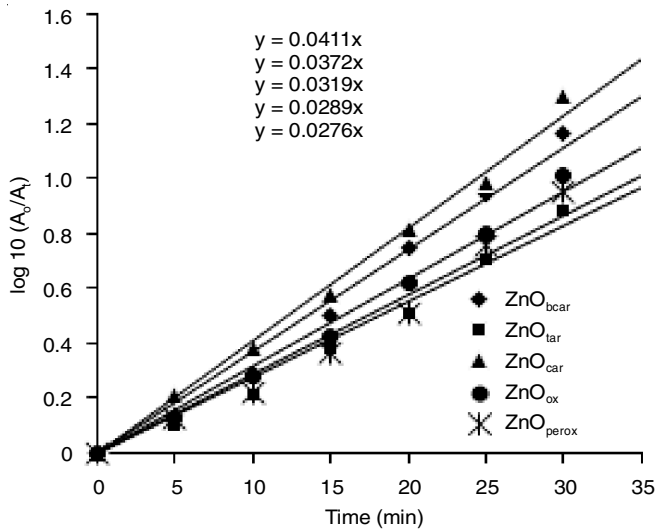


Fig. 7. Kinetics of the decolorization of crystal violet dye in sunlight

Owing to larger crystallite size and lower specific surface area (Table-2) of  $\text{ZnO}_{\text{car}}$  exhibited better photocatalytic activity than  $\text{ZnO}_{\text{perox}}$  sample, which can be attributed to its granular structure. SEM images clearly illustrated that  $\text{ZnO}_{\text{car}}$ ,  $\text{ZnO}_{\text{bcar}}$  and  $\text{ZnO}_{\text{tar}}$  samples had less agglomeration of grains while  $\text{ZnO}_{\text{ox}}$  and  $\text{ZnO}_{\text{perox}}$  samples showed higher agglomeration of grains. The photoluminescence spectrum of  $\text{ZnO}_{\text{perox}}$  showed a comparatively high intensities of peak indicated that rate of recombination of electron-hole pair was high in this sample. Thus, though  $\text{ZnO}_{\text{perox}}$  sample had higher specific surface area but displayed lower photocatalytic activity. A  $\text{ZnO}_{\text{tar}}$  sample did not show high agglomeration due to larger size of grains therefore had a lower specific surface area. Thereby, this photocatalyst exhibited the lowest photocatalytic activity. The surface of  $\text{ZnO}_{\text{car}}$  grains appeared rough which results in more adsorption of dye molecules at the surface.

**Photocatalytic mineralization of dye from effluent:** The dye effluent samples were collected from small scale fabric dyeing unit located at Malegaon city, India. Samples were characterized using  $\text{ZnO}_{\text{car}}$  photocatalyst (Table-3, Fig. 8). The collected effluents showed alkaline pH, which indicated the use of caustic soda in the preparation of dye solution for dyeing purposes. The photocatalytic degradation of dyes from effluents was carried out without further adjustment of pH. The mineralization is different from decolorization. The decolorization takes place due to fragmentation of molecule while in mineralization dye molecule is completely decomposed to  $\text{CO}_2$  and  $\text{H}_2\text{O}$  [24]. The decolorization of dye effluent is confirmed by recording the absorbance at  $\lambda_{\text{max}}$  of dye effluent. The decolourized dye effluent showed a very high UV absorbance (Fig. 9), which indicated that dye effluent was colourless and contains UV absorbing fragments of dye molecule. Thus, degradation experiment was continued till UV absorbance becomes negli-

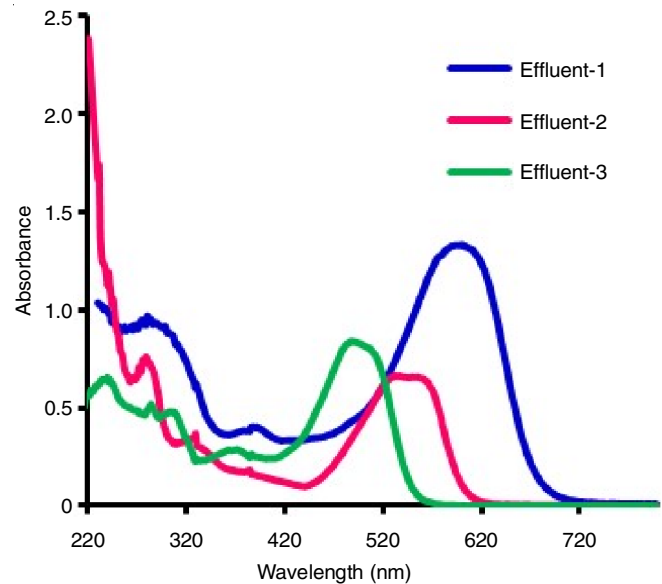


Fig. 8. UV-visible spectra of the effluents

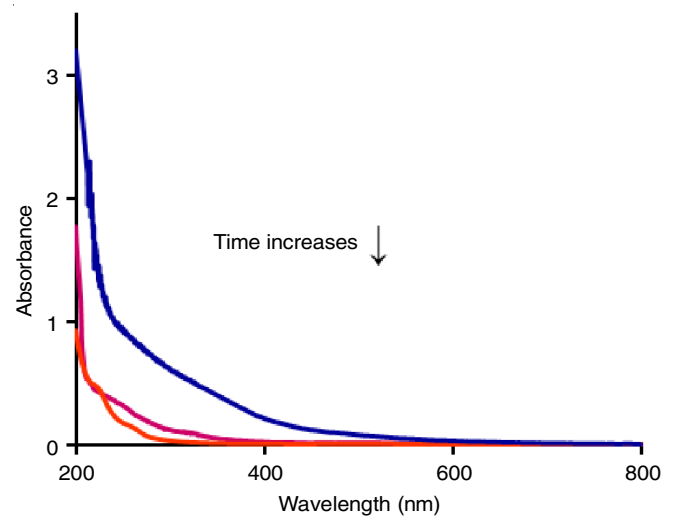


Fig. 9. Absorbance spectra effluent-3 at 60 (decolorization stage), 120 and 180 min time of irradiation

gible. It required about 180 min for effluent-1 and 250 min for effluent-2 and 3. All three effluents showed more than 95% COD removal (Table-3) after 250 min of irradiation time.

#### CONFLICT OF INTEREST

The authors are grateful to DST, Government of India, for awarding the research grant (Ref. DST-FIST, SR/FST/College-224/2014).

#### CONFLICT OF INTEREST

The authors declare that there is no conflict of interests regarding the publication of this article.

TABLE-3  
CHARACTERISTICS OF DYE EFFLUENT PERCENT COD REMOVAL

Effluent No.	Colour of the effluent	Absorbance maxima (nm)	pH	COD (ppm)	Time of complete decolourization (min)	Effluent treatment time (min)	COD removal (%)
1	Blue	605	8.7	107 ± 8	40	180	96.25 ± 4.7
2	Red-violet	550	8.3	68 ± 11	75	250	98.83 ± 3.6
3	Orange	490	8.4	79 ± 6	60	250	97.06 ± 4.3

## REFERENCES

1. M.A. Ali, M.R. Idris and E.M. Quayum, *J. Nanostr. Chem.*, **3**, 36 (2013); <https://doi.org/10.1186/2193-8865-3-36>
2. D.R. Shinde, P.S. Tambade, M.G. Chaskar and K.M. Gadave, *Drink. Water Eng. Sci.*, **10**, 109 (2017); <https://doi.org/10.5194/dwes-10-109-2017>
3. J. Zhang, S.J. Deng, S.Y. Liu, J.M. Chen, B.Q. Han, Y. Wang and Y.D. Wang, *Adv. Perform. Mater.*, **29**, 263 (2014).
4. M. Thirumavalavan, F.M. Yang and J.F. Lee, *Environ. Sci. Pollut. Res. Int.*, **20**, 5654 (2013); <https://doi.org/10.1007/s11356-013-1575-3>
5. O. Bechambi, M. Chalbi, W. Najjar and S. Sayadi, *Appl. Surf. Sci.*, **347**, 414 (2015); <https://doi.org/10.1016/j.apsusc.2015.03.049>
6. A. Abdel Aal, S.A. Mahmoud and A.K. Aboul-Gheit, *Nanoscale Res. Lett.*, **4**, 627 (2009); <https://doi.org/10.1007/s11671-009-9290-1>
7. O.J. Perales-Perez, M.S. Tomar, S.P. Singh, A. Watanabe, T. Arai, A. Kasuya and K. Tohji, *Phys. Status Solidi*, **1**, 803 (2004); <https://doi.org/10.1002/pssc.200304266>
8. W. Shen, A. Li, H. Wang, Y. Liu, W. Guo and Y. Zhang, *J. Hazard. Mater.*, **152**, 172 (2008); <https://doi.org/10.1016/j.jhazmat.2007.06.082>
9. R.Y. Hong, J.H. Li, L.L. Chen, D.Q. Liu, H.Z. Li, Y. Zheng and J. Ding, *Powder Technol.*, **189**, 426 (2009); <https://doi.org/10.1016/j.powtec.2008.07.004>
10. A. Dodd, A. McKinley, T. Tsuzuki and M. Saunders, *J. Nanopart. Res.*, **10(S1)**, 243 (2008); <https://doi.org/10.1007/s11051-008-9412-1>
11. L. Shen, N. Bao, K. Yanagisawa, K. Domen, A. Gupta and C.A. Grimes, *Nanotechnology*, **17**, 5117 (2006); <https://doi.org/10.1088/0957-4484/17/20/013>
12. R.A. Pawar, D.R. Shinde and P.S. Tambade, *Desalination Water Treat.*, **57**, 16514 (2016); <https://doi.org/10.1080/19443994.2015.1079248>
13. B.S. Furniss, A.J. Hannaford, P.W.G. Smith and A.R. Tatchell, Vogel, *Textbook of Practical Organic Chemistry*, ELBS: London, edn 5 (1989).
14. I.H. Gul, A.Z. Abbasi, F. Amin, M. Anis-ur-Rehman and A. Maqsood, *J. Magnet. Magn. Mater.*, **311**, 494 (2007); <https://doi.org/10.1016/j.jmmm.2006.08.005>
15. J. Antony, J. Nutting, D.R. Baer, D. Meyer, A. Sharma and Y. Qiang, *J. Nanomater.*, **2006**, 54961 (2006); <https://doi.org/10.1155/JNM/2006/54961>
16. M.N. Chong, B. Jin, C.W.K. Chow and C.P. Saint, *Chem. Eng. J.*, **152**, 158 (2009); <https://doi.org/10.1016/j.cej.2009.04.027>
17. X. Chu, T. Chen, W. Zhang, B. Zheng and H. Shui, *Sens. Actuators B Chem.*, **142**, 49 (2009); <https://doi.org/10.1016/j.snb.2009.07.049>
18. P. Hu, N. Han, D. Zhang, C.H. Johnny and Y. Chen, *Sens. Actuators B Chem.*, **169**, 74 (2012); <https://doi.org/10.1016/j.snb.2012.03.035>
19. M. Poloju, N. Jayababu and M.V. Ramana Reddy, *Mater. Sci. Eng. B*, **227**, 61 (2018); <https://doi.org/10.1016/j.mseb.2017.10.012>
20. N.K. Singh, S. Saha and A. Pal, *Desalination Water Treat.*, **53**, 501 (2015); <https://doi.org/10.1080/19443994.2013.838520>
21. L. Xu, B. Wei, W. Liu, H. Zhang, C. Su and J. Che, *J. Nano. Res. Lett.*, **8**, 536 (2013); <https://doi.org/10.1186/1556-276X-8-536>
22. L. Duan, B. Lin, W. Zhang, S. Zhong and Z. Fu, *Appl. Phys. Lett.*, **88**, 232110 (2006); <https://doi.org/10.1063/1.2211053>
23. B.J. Niu, L.L. Wu, W. Tang, X.T. Zhang and Q.G. Meng, *CrystEngComm*, **13**, 3678 (2011); <https://doi.org/10.1039/c1ce05175j>
24. N.A. Yusoff, L.N. Ho, S.A. Ong, Y.S. Wong and W.F. Khalik, *Desalination Water Treat.*, **57**, 12496 (2016); <https://doi.org/10.1080/19443994.2015.1054312>
25. M. Shanthi and V. Kuzhalosai, *Indian J. Chem.*, **51A**, 428 (2012).
26. T.F. Sampaio, I.A. Guerrini, X.L. Otero, F.M. Vazquez, J.C. Bogiani, F.C. Oliveira, J.L. Gava, M.A. Ciol, K.M. Littke and R.B. Harrison, *Water Air Soil Pollut.*, **227**, 1 (2016); <https://doi.org/10.1007/s11270-015-2689-7>